Proc. Natl. Acad. Sci. USA
Vol. 95, pp. 3408–3412, March 1998
Biochemistry

Crystal structure of the catalytic domain of human tumor necrosis factor-α-converting enzyme

KLAUS MASKOS*†, CARLOS FERNANDEZ-CATALAN*†, ROBERT HUBER*, GLEB P. BOURENKOV‡, HANS BARTUNIK‡, GEORGE A. ELLESTAD§, PRANITHA REDDY¶, MARTIN F. WOLFSON¶, CHARLES T. RAUCH¶, BEVERLY J. CASTNER¶, RAYMOND DAVIS¶, HOWARD R. G. CLARKE¶, MELISSA PETERSEN¶, JEFFREY N. FITZNER¶, DOUGLAS PAT CERRETTI¶, CARL J. MARCH¶, RAYMOND J. PAXTON¶, ROY A. BLACK¶, AND WOLFRAM BODE*‖

*Max-Planck-Institut für Biochemie, D-82152 Martinsried, Germany; ‡AG Proteindynamik MPG-ASMB c/o DESY, D-22603 Hamburg, Germany; §Wyeth–Ayerst Research, Pearl River, NY 10965; and ¶Immunex Corporation, Seattle, WA 98101

Contributed by Robert Huber, January 12, 1998

ABSTRACT **Tumor necrosis factor-α (TNFα) is a cytokine that induces protective inflammatory reactions and kills tumor cells but also causes severe damage when produced in excess, as in rheumatoid arthritis and septic shock. Soluble TNFα is released from its membrane-bound precursor by a membrane-anchored proteinase, recently identified as a multidomain metalloproteinase called TNFα-converting enzyme or TACE. We have cocrystallized the catalytic domain of TACE with a hydroxamic acid inhibitor and have solved its 2.0 Å crystal structure. This structure reveals a polypeptide fold and a catalytic zinc environment resembling that of the snake venom metalloproteinases, identifying TACE as a member of the adamalysin/ADAM family. However, a number of large insertion loops generate unique surface features. The pro-TNFα cleavage site fits to the active site of TACE but seems also to be determined by its position relative to the base of the compact trimeric TNFα cone. The active-site cleft of TACE shares properties with the matrix metalloproteinases but exhibits unique features such as a deep S3′ pocket merging with the S1′ specificity pocket below the surface. The structure thus opens a different approach toward the design of specific synthetic TACE inhibitors, which could act as effective therapeutic agents *in vivo* to modulate TNFα-induced pathophysiological effects, and might also help to control related shedding processes.**

Tumor necrosis factor-α (TNFα) (1), a major immunomodulatory and proinflammatory cytokine, is synthesized as a 223-aa membrane-anchored precursor. The soluble form of TNFα, comprising the C-terminal two-thirds of this precursor, is released into extracellular space by limited proteolysis at the Ala-76 → Val-77 bond. The proteinase responsible for this cleavage, called TACE or ADAM 17, has recently been identified (2, 3) as a zinc-endopeptidase consisting of a multidomain extracellular part, an apparent transmembrane helix and an intracellular C-terminal tail. The extracellular part comprises an N-terminal pro domain, a 259-residue catalytic domain, and a Cys-rich moiety that has been hypothesized to be composed of a disintegrin-like, an epidermal growth factor-like, and a crambin-like domain (2). Its polypeptide sequence, in particular, that accounting for the catalytic domain, indicates some similarity with other metzincins (4, 5), especially with the adamalysins/ADAMs (6–8) (a protein family comprising snake venom metalloproteinases and membrane-anchored surface proteins containing an adamalysin-like catalytic domain) and the matrix metalloproteinases (MMPs). In comparison to enzymes in these families, however, the polypeptide chain of the TACE catalytic domain is clearly longer and is stable in the absence of calcium. Further, in contrast to the MMPs, TACE is relatively insensitive to the tissue inhibitor of metalloproteinases-1 (TIMP-1) (9) and exhibits a different inhibition pattern toward synthetic inhibitors (9–12). In contrast to the MMPs, TACE cleaves a 12-mer peptide spanning the cleavage site in pro-TNFα selectively between Ala and Val (9). TNFα has been implicated in various deleterious physiological conditions such as rheumatoid arthritis, cachexia, and endotoxic shock; thus, blocking its release into the circulation by inhibitors might provide major therapeutic benefits (10–13).

We have undertaken an x-ray crystal structure analysis of the catalytic domain of TACE. This experimental model clarifies the structural and evolutionary relationships of TACE to other metzincins and will allow the structure-based design of TACE inhibitors capable of discriminating against other structurally related enzymes.

MATERIALS AND METHODS

A DNA construct encoding the pro and the catalytic domain of human TACE (residues 1–477), with Ser-266 changed to Ala and Asn-452 to Gln to prevent N-linked glycosylation, and with the sequence Gly-Ser-$(His)_6$ added to the C terminus to facilitate purification, was expressed in CHO cells (R.A.B., unpublished data). These cells primarily secreted processed TACE, about half of which began with Val-212 and half with Arg-215. This mature proteinase mixture was purified by NTA-Ni affinity chromatography followed by gel filtration, and was cocrystallized with the Immunex compound 3, *N*-{D,L-[2-(hydroxyamino-carbonyl)methyl]-4-methylpentanoyl}L-3-(tert-butyl)glycyl-L-alanine at room temperature in about 20% isopropanol, 20% PEG4000, and 0.1 M citrate, pH 5.4, by using the sitting drop vapor diffusion technique. These crystals belong to the monoclinic space group P 2_1, have cell constants a = 61.38 Å, b = 126.27 Å, c = 81.27 Å, β = 107.41°, and contain four molecules in the asymmetric unit.

Anomalous diffraction data to 2.0 Å were collected with a MAR345 imaging plate scanner at 100 K on the BW6 wiggler beam line of DORIS (Deutsches Elektronen Synchrotron, Hamburg, Germany), by using monochromatic x-ray radiation at the wavelengths of maximal f″ (1.2769 Å) and minimal f′

The publication costs of this article were defrayed in part by page charge payment. This article must therefore be hereby marked "*advertisement*" in accordance with 18 U.S.C. §1734 solely to indicate this fact.

Abbreviations: TNFα, tumor necrosis factor-α; TACE, TNFα converting enzyme; ADAM, a disintegrin and metalloprotease; MMP, matrix metalloproteinase; TIMP, tissue inhibitor of metalloproteinase.

Data deposition: The atomic coordinates and structure factors have been deposited at the Protein Data Bank, Biology Department, Brookhaven National Laboratory, Upton, NY 11973 (accession no. BNL-21333).

†K.M. and C.F.-C. contributed equally to this work.

‖To whom reprint requests should be addressed. e-mail: bode@biochem.mpg.de.

(1.2776 Å) at the K absorption edge of zinc and at a remote wavelength (1.060 Å). These data were evaluated and scanned by using DENZO/SCALEPACK (14), yielding 77,653 independent reflections from 1,051,836 measurements (96.9% completeness, *R*-merge 0.031 in intensities).

All attempts to solve the crystal structure by Patterson search/molecular replacement methods by using modified adamalysin models failed to give useful starting positions for phasing. Thus, the four independent zinc atoms were located from an anomalous difference Patterson synthesis. Multiple wavelength anomalous diffraction phases were refined (yielding 5.0 and −5.1 electrons for f″ and f′ at 1.2769 Å, and 2.6 and −9.0 electrons for f″ and f′ at 1.2776 Å) and calculated with MLPHARE (15) including all measured data to 2.0 Å resolution. Their initial mean-figure-of-merit of 0.53 was increased to 0.76 by solvent flattening/histogram matching methods applying the program DM (16). This density allowed building of the complete chains of the four independent TACE catalytic domains and the bound hydroxamic acid inhibitors on an SGI graphic station by using TURBO-FRODO (17). This model was crystallographically refined with XPLOR (18) and with REFMAC (19) without applying any noncrystallographic symmetry restraints.

Molecules 1 and 3 and 2 and 4 are defined from Asp-219 and Met-221, respectively, to Ser-474. The *R* factor of the model, comprising, besides the 4 protein molecules, 4 inhibitor molecules, 172 solvent molecules, and 4 zinc ions, is 18.6% (*R*-free, 27.4%) for 71,400 independent reflections from 12.0 to 2.0 Å resolution. The rms deviation from target bond values is 0.015 Å. Omitting 10 to 15 residues, the molecules show rms deviations of 0.22 (molecules 1 with 3, and 2 with 4) to 0.40 Å (the residual combinations), values close to the estimated experimental error. Considerable shifts are only visible in a few surface loops, in particular in the second "ear."

RESULTS AND DISCUSSION

The monoclinic crystals contain four molecules in the crystallographic asymmetric unit. The molecules are not arranged as separate symmetric tetramers, but form an infinite periodic structure without a transition. In spite of quite different crystal contacts, the four molecules have, except for shifts of a few surface loops, very similar structures allowing a common description of the essential structural features.

The TACE catalytic domain (Fig. 1) has the shape of an oblate ellipsoid, notched at its flat side to give a relatively small active-site cleft separating a small "lower" subdomain from an "upper" main molecular body (Fig. 2*b*). Central to it is a highly twisted, five-stranded β-pleated sheet (strands sI–sV, see Figs. 1 and 3) flanked on its convex side by α-helices hB and hB2 and on its concave side by helices hA and hC. β-strands sII and sIII are linked by a large "multiple-turn loop," a long "intermediate" α-helix (hB), and an adjacent short α-helix (hB2), all arranged on "top" of the β-sheet and thus fully shielding its central part from bulk water (Fig. 1). The multiple-turn loop is bulged out at two sites, giving rise to a "spur-like" and an "acidic" protuberance (visible in Fig. 2*b* on top of the molecule). The sIII–sIV linker terminates in a short "bulge" before entering the "edge" strand sIV, the only antiparallel β-strand. The sIV–sV connecting segment is dissected into two large "ear-like" surface loops, the first one nestling to the main molecular body (giving rise to the "blue" surface, center left in Fig. 2*b*), and a long β-hairpin loop (sIVa–sIVb) projecting from the molecular surface (upper left in Figs. 1 and 2*b*). A bulged-out loop links sV with the "active-site helix" hC, which is located in the center of the molecule and stops abruptly at the strictly conserved Gly-412. At this point, the chain kinks down to build the lower subdomain.

The C-terminal chain comprising the last 61 residues of the TACE catalytic domain (Fig. 3) first forms three short,

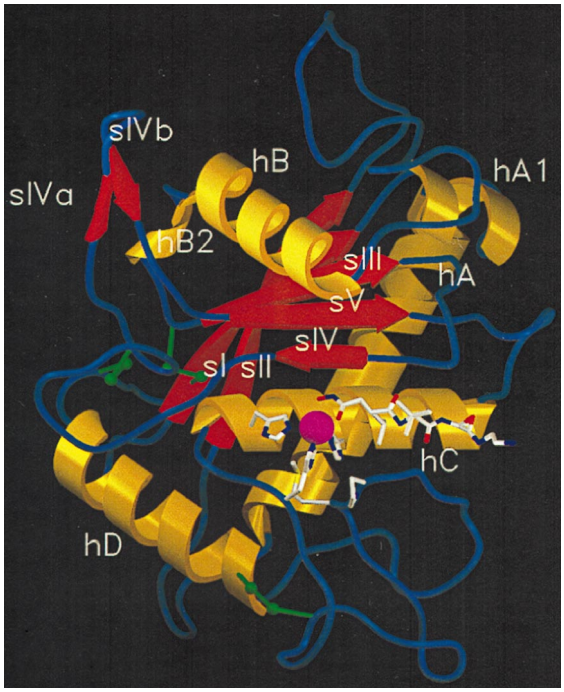

FIG. 1. Ribbon diagram of the TACE catalytic domain. The chain starts and ends on the lower and upper left backside, respectively. The three disulfides are shown as green connections and the catalytic zinc is shown as a pink sphere. His-405, His-409, His-415, Met-435, Pro-437, and the inhibitor (white) are shown with their full structure. The figure was made with SETOR (20).

straight, almost perpendicularly arranged segments linked by two "narrow," super-twisted loops. From there it returns via the tight "Met-turn" Tyr-433 → Val-434 → Met-435 → Tyr-436 back to the surface where it kinks at Pro-437 to form the Pro-437 → Ile-438 → Ala-439 outer "wall" of the S1′ crevice. Then, a wide loop precedes the C-terminal α-helix hD, after which the chain ends up on the molecular "back" surface close to the N terminus (Fig. 1). The first of the two "narrow" loops is disulfide-linked via Cys-423 → Cys-453 to the N terminus of helix hD. The C-terminal end of this helix is clamped to the "ear-like" sIV–sV linker peptide through Cys-365 → Cys-469. The spatially adjacent third disulfide bridge, Cys-225 → Cys-333, connects the N-terminal parts of β-strands sI and sIII. The last defined residues, Arg-473 and Ser-474, are fixed via hydrogen bonds to the main molecular body. In the intact TACE molecule, the following (presumably disintegrin-like) domain would probably pack to the "left back" surface side of the catalytic domain (see Fig. 5).

The active-site cleft of TACE (see Fig. 5) is relatively flat on the left-hand (nonprimed) side but becomes notched toward the right. The catalytic zinc residing in its center is pentacoordinated by the three imidazole Nε2 atoms of His-405, His-409, and His-415 (provided by the active-site helix and the following "descending" chain, together comprising the conserved zinc-binding consensus motif HEXXHXXGXXH) and by the carbonyl and the hydroxyl oxygens of the inhibitor's hydroxamic acid moiety, which presumably displaces a water molecule in the active enzyme (Figs. 4 and 5). This zinc-imidazole ensemble is placed above the distal ε-methyl-sulfur moiety of the strictly conserved Met-435, found in the Met-turn characteristic of the metzincin clan (5). Both carboxylate oxygens of the "catalytic" Glu-406 [which acts as a general base during catalysis (24)], squeezed between the zinc-liganding imidazole of His-405 and the edge strand, are hydrogen bonded to the hydroxyl and the N—H group of the hydroxamic acid (Fig. 4). Immediately to the right of the catalytic zinc invaginates the medium-sized, essentially hydrophobic, S1′

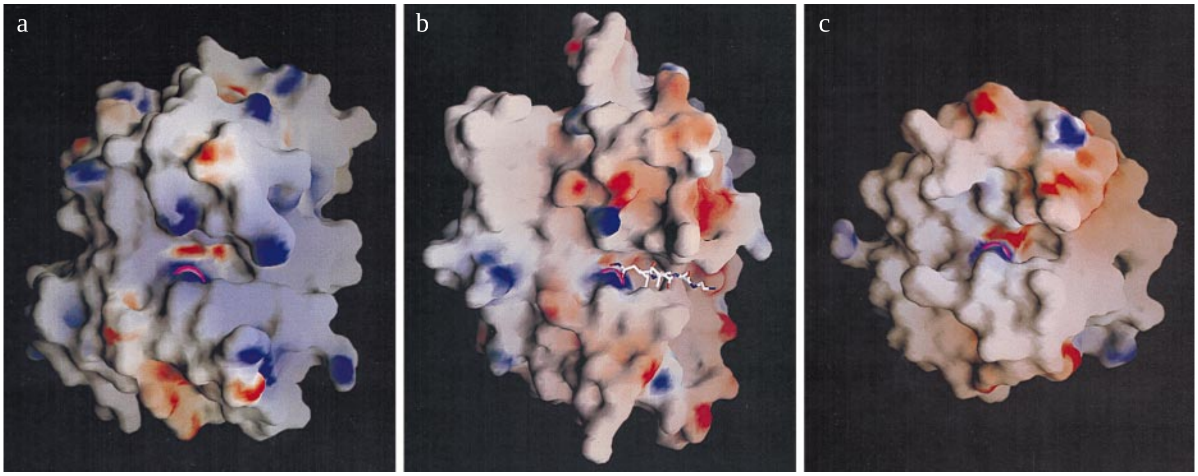

FIG. 2. Solid-surface representations of the catalytic domains of adamalysin II (6, 7) (*a*), TACE (*b*), and MMP-3 (*d*) (21). The electrostatic surface potentials are contoured from −20 (intense red) to 20 k_BT/e (intense blue). The active-site clefts run from left to right, with the catalytic zinc atoms (pink spheres) in the centers. In TACE, the bound inhibitor is shown in full structure. Orientations are equivalent to Fig. 1. The figure was made with GRASP (22).

specificity pocket (Figs. 2*b* and 5). Further to the right opens through a polar entrance a second hydrophobic (S3′) pocket, which merges inside the molecule with the S1′ pocket bridged by the opposing side chains of Ala-439 and Leu-348.

The (pseudo)peptidic part of the inhibitor binds in an extended geometry to the notched right-hand side of the active-site cleft, mimicking the interaction of the primed residues of a productively bound peptide substrate (Fig. 5). It runs antiparallel to the upper short bulge Gly-346 → Thr-347 → Leu-348 and parallel to the S1′ wall segment, forming two intermain-chain hydrogen bonds with each of them. The dominant intermolecular interactions are made by the P1′ isobutyl (pseudo-leucyl) side chain of the inhibitor and the hydrophobic bottleneck to the S1′ pocket, which accommodates three additional solvent molecules linked through a water channel to the adjacent S3′ pocket. The P2′ t-butyl side chain extends away from the enzyme, but nestles against the hydrophobic canopy formed by the enzyme's bulge. The P3′ Ala side chain points to the large S3′ pocket, but is too short to make favorable contacts. The C-terminal diaminoethyl group extends away from the cleft, adapting two different conformations in the four molecules.

The P1′ to P3′ segment Val-77 → Arg-78 → Ser-79 of a bound pro-TNFα will probably bind to TACE in a similar manner, with the isopropyl side chain of Val-77 just fitting into the hydrophobic S1′ neck, the Arg-78 side chain anchoring to the carbonyl and hydroxyl groups at the upper rim, and the Ser-79 hydroxyl interacting with the polar entrance to the S3′ pocket. The preceding P3 to P1 pro-TNFα residues Ala-74 → Gln-75 → Ala-76 most likely will align antiparallel to the edge strand, with their side chains extending into the S3 pocket and the (polar) shallow S2 depression, and projecting out of the

```
                                                     sI          hA1
                                                 →→→→→→||||||||||||
ADAM_CROAD       .......... ......EQNL PQRYIELVVV ADRRVFMKYN
TACE         205 PEELVHR... .VKRRADPDP MKNTCKLLVV ADHRFYRYMG 240
hADAM10          QEKHAINGPE LLRKRRTTSA EKNTCQLYIQ TDHLFFKYYG

                        hA                             sII
                 ||||||||||||||||||||||||||||||       →→→→
ADAM_CROAD       .SDLNIIRTR VHEIVNIINE FYRSL..... ...NIRVSLT
TACE         241 RGEESTTTNY LIELIDRVDD IYRNTSWDNA GFKGYGIQIE 280
hADAM10          TRE..AVIAQ ISSHVKAIDT IYQTT..DFS GIRNISFMVK

                  sII                                  hB
                 →→→                             ||||||||||||
ADAM_CROAD       DLEIWSGQDF I......TI. .......... QSSSSNTLNS
TACE         281 QIRILKSPQE VKPGEKHYNM AKSYPNEEKD AWDVKMLLEQ 320
hADAM10          RIRINTTADE KDPTNPF... ..RFPN.... .ISVEKFLE.

                  hB   hB2         sIII            sIV
                 ||||| ||||||||    →→→→→           →→→
ADAM_CROAD       FGEWRERVLL TRKRHDNAQL LTAINFEGKI IGKAYTS...
TACE         321 FSFDIAEEAS ...KVCLAHL FTYQDFDMGT LGLAYVGSPR 357
hADAM10          ..LNSEQNHD ...DYCLAYV FTDRDFDDGV LGLAWVGAP.

                            sIVa   sIVb      sV            hC
                             →→     →→     →→→→           ||||
ADAM_CROAD       .....SMCNP .......... .RSSVGIVKD HSP....INL
TACE         358 ANSHGGVCPK AYYSPVGKKN IYLNSGLTST KNYGKTILTK 397
hADAM10          SGSSGGICEK SKLYSDGKKK .SLNTGIITV QNYGSHVPPK

                           hC
                 ||||||||||||||||||||||||
ADAM_CROAD       LVAVTMAHEL GHNLGMEHDG K....DCLRG ........AS
TACE         398 EADLVTTHEL GHNFGAEHDP DGLAECAPNE D......QGG 431
hADAM10          VSHITFAHEV GHNFGSPHDS G..TECTPGE SKNLGQKENG

                                              hD
                                  ||||||||||||||||||||||||||
ADAM_CROAD       LCIMRPGLTP GRS...YEFS DDSMGYYQKF LNQYKPQCIL
TACE         432 KYVMYPIAVS GDHENNKMFS NCSKQSIYKT IESKAQECFQ 471
hADAM10          NYIMYARATS GDKLNNNKFS LCSIRNISQV LEKKRNNCFV

ADAM_CROAD       NKP....... ..........
TACE         472 ERSNKVCGNS RVDEGEECDP 491
hADAM10          ESGQPICGNG MVEQGEECDC
```

FIG. 3. Alignment of the catalytic domain sequences of adamalysin II (ADAM_CROAD) (7) and human ADAM 10 (hADAM10) (23) with TACE (2, 3). These sequences were aligned according to their topological equivalence and visually, respectively. Residue numbering is made according to the coded TACE sequence. Arrows and braces represent β-strands and α-helices in TACE. Blue symbols indicate topologically nonequivalent residues of adamalysin and TACE, and red designates residues that are identical in all three proteinases.

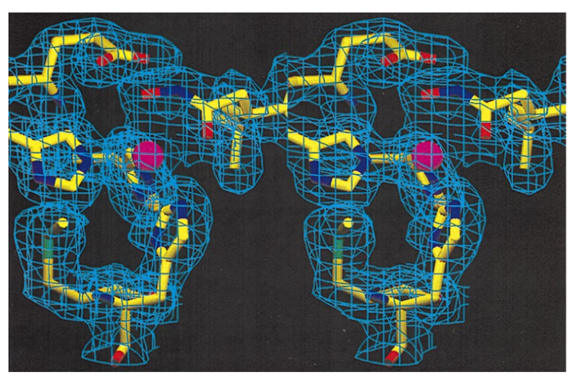

FIG. 4. Stereo section of the final 2.0 Å electron density around the catalytic zinc (pink sphere) superimposed with the final TACE model (with His-405 in the back, Glu-406 and the hydroxamic acid inhibitor moiety on top, His-409 to the left, and Met-435 and His-415 at the bottom). The average Zn—N or O distances are 2.3 Å. Orientation is similar to Fig. 1. Figure was made with TURBO-FRODO (17).

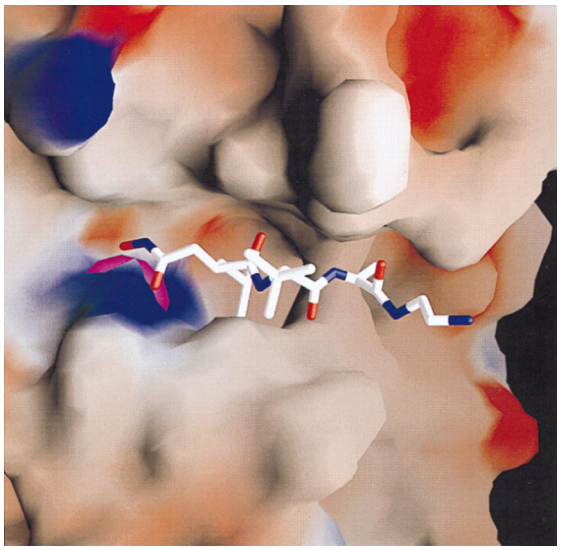

FIG. 5. Close-up view of the active-site cleft of TACE. On top of the solid surface representing the proteinase the bound inhibitor is shown in full structure, slotting with its isobutyl (P1′) and its Ala (P3′) side chains into the deep S1′ and the novel S3′ pockets. Figure was made as Fig. 2*b* (22).

(hydrophobic) cleft, respectively (Fig. 5). Thus, the preferential pro-TNFα cleavage at Ala-76 → Val-77 by TACE can partly be explained by favorable interactions in the active-site vicinity. Experimental evidence (25–27) suggests, however, that the cleavage site is also determined by its arrangement relative to the base of the compact cone (28) formed by the associated C-terminal segments of three pro-TNFα molecules (25). Preliminary docking experiments show, in fact, that the base of this TNFα-trimer cone [into which the six to eight disordered N-terminal TNFα residues ascend (28)] might be specifically recognized by the "right" side of the TACE catalytic domain, so that the pro-TNFα cleavage segment would precisely lock with its Ala-76 → Val-77 pair into the active site of TACE (Fig. 6). In addition, the processing of the membrane-bound pro-TNFα by TACE *in vivo* might be guided

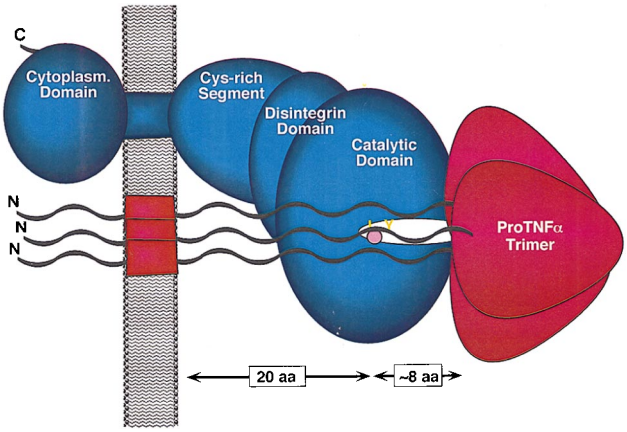

FIG. 6. Schematic model of the hypothetical pro-TNFα–TACE complex. The full-length activated TACE consists of the catalytic domain (shown in standard orientation, Fig. 1), a disintegrin-like domain, a Cys-rich moiety, the transmembrane segment, and the intracellular domain. The trimeric pro-TNFα consists of intracellular segments, transmembrane segments, 26–28 residue spacers forming a stalk, and the compact trimeric TNFα cone (28). TACE and pro-TNFα might be anchored in the membrane in such a manner that the TNFα cone is attached to the "right" side of the catalytic domain, with the scissile Ala-76 → Val-77 bond of one extended pro-TNFα strand placed above the active site.

by assembling, i.e., by the mode of presentation of the [presumably nonstructured (26)] pro-TNFα cleavage segment to the TACE active site at a defined distance from the anchoring membrane.

The polypeptide topology and in particular the surface presentation of the catalytic zinc reveal the catalytic domain of TACE to be a typical metzincin (4, 5), with closest similarities to the catalytic domain of snake venom metalloproteinases such as adamalysin II (6, 7, 29, 30) (Figs. 2*a* and 7). The close structural similarity is reflected by the superposition of the central β-sheet and the long α-helices and, in particularly, by a number of structural features that TACE shares exclusively with the adamalysins: the long helix hB and the preceding multiple-turn loop arranged on top of the β-sheet; the typically arranged and shaped C-terminal helix hD; and the extended C terminus placed on the backside surface. About 175 of the 259 TACE and 201 adamalysin residues are topologically equivalent (with a Cα-atom rms deviation of 1.3 Å), and 39 of them are identical (see Fig. 3). Additional structural features that confirm the close relationship of TACE to the adamalysins include: the loosely arranged N terminus; the characteristic Asp-416 (directly following the zinc-binding consensus motif, Fig. 3) involved in identical intramolecular hydrogen bond interactions; the adjacent disulfide bridge Cys-423 → Cys-453 linking the first narrow loop to the C-terminal helix hD [which TACE does not share with adamalysin II or atrolysin, but with the H2-proteinase from the snake venom of *Trimeresurus flavoviridis* (30)]; and disulfide bridge Cys-365 → Cys-469 connecting the sIV–sV linker with the C-terminal helix hD.

However, the catalytic domain of TACE also differs from adamalysin in several respects: with 259 residues, its chain is much longer; most of the additional residues of TACE are clustered, giving rise to the two surface protuberances of the multiple-turn loop, to the two "ears" of the sIV–sV linker, and to a more bulged-out sV-hC connector (see Figs. 3 and 7); TACE lacks an adamalysin-like calcium-binding site (though the disulfide bridge Cys-225 → Cys-333 in TACE serves the

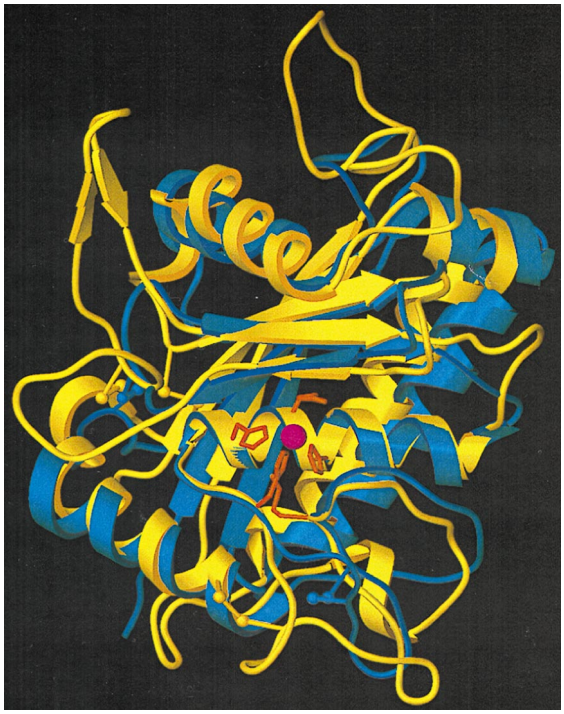

FIG. 7. Superposition of the ribbons of the catalytic domain of TACE (gold) and adamalysin (blue) (6, 7). Also shown are the catalytic zinc of TACE (pink sphere) and the three (TACE) and two (adamalysin) disulfide bridges. Orientation is similar to Fig. 1. Figure was made with GRASP (22).

same function clamping the N-terminal chain to strand sIII); TACE has a deep S3′ pocket merging with its S1′ pocket; and the charge pattern in and around the primed subsites is inverted in TACE compared with adamalysin (Fig. 2 *a* and *b*).

This structure thus shows that TACE is not a typical member of the mammalian ADAMs but stands outside. TACE shares this role with ADAM 10, for which a TACE-like specificity has been demonstrated (23, 31) and whose *Drosophila* version (kuz) has recently been shown to process the transmembrane receptor Notch (32). ADAM 10, too, probably exhibits an elongated hA-sII loop and the two "ears" found in TACE, but might have a multiple-turn intermediate in size between TACE and adamalysin. Ninety-one of the ADAM 10 catalytic domain residues are identical to TACE (Fig. 3). The other mammalian ADAMs, in contrast, probably resemble adamalysin II much more closely (see ref. 7).

The structural homology between the catalytic domains of TACE and the MMPs is significantly lower. The relative arrangement of the common secondary structural elements differs more (reflected by the significantly larger rms deviation of 1.6 Å of the approximately 120 topologically equivalent Cα-atoms), and the MMPs lack characteristic TACE/adamalysin structural elements (such as the intermediate helix hB and the multiple-turn loop, the Asp residue following the third zinc-binding histidine) or exhibit common features (such as the structural zinc and the integrated calcium ions) not seen in TACE. Notwithstanding the obvious differences in secondary structure, the active-site cleft of TACE bears some similarity to that of the MMPs, with the flat, nonprimed (left-hand) side, and the narrow primed side centering around the S1′ pocket of varying size (Fig. 2 *b* and *c*). This subsite similarity to the MMPs explains the observed sensitivity of a TACE-like activity to synthetic hydroxamic acid inhibitors originally designed for inhibition of various MMPs (11). Model building experiments with the TIMP-1 structure (21) show no obvious steric interference in the active-site region that could explain why TACE is insensitive to the TIMPs (9); more detailed studies will hopefully allow the design of TIMP-variants with improved affinity for TACE in the near future.

This TACE crystal structure thus gives evidence for a substantial topological similarity between the catalytic domains of TACE and the adamalysins/ADAMs, and it shows that TACE's substrate-binding site resembles that of the MMPs. TACE exhibits, however, several structural peculiarities regarding surface charge and shape, which may enable the design of potent selective synthetic inhibitors. Such tailored inhibitors could be of wide use to study the physiological role of TACE, as well as that of TNFα, but, in particular, could also become valuable therapeutics of arthritic lesions and may increase the rate of survival in various endotoxin-induced septic shock syndromes (10). Such tailored inhibitors might clarify the role of TACE in the processing of other members of the TNF superfamily and in the shedding of a number of other cell surface proteins (12, 33).

We thank Mrs. M. Braun for excellent assistance with crystallization, J. Medrano for computing advice, R. Johnson, M. Gerhart, and M. DeJardin for protein analyses, and A. Woodward and B. Rasmussen for growing the CHO cells. The financial support by the SFB469, the Biotechnology Program (contract ERBBIO4-CT960464) of the European Union, the Bundesministerium für Bildung und Forschung, and the Fonds der Chemischen Industrie is kindly acknowledged.

1. Bemelmans, M. H. A., VanTits, L. J. H. & Buurman, W. A. (1996) *Crit. Rev. Immunol.* **16,** 1–11.
2. Black, R. A., Rauch, C. T., Kozlosky, C. J., Peschon, J. J., Slack, J. L., Wolfson, M. F., Castner, B. J., Stocking, K. L., Reddy, P., Srinivasan, S., *et al.* (1997) *Nature (London)* **385,** 729–733.
3. Moss, M. L., Jin, S. L. C., Milla, M. E., Burkhart, W., Carter, H. L., Chen, W. J., Clay, W. C., Didsberg, J. R., Hassler, D., Hoffman, C. R., *et al*. (1997) *Nature (London)* **385,** 733–736.
4. Bode, W., Gomis-Rüth, F.-X. & Stöcker, W. (1993) *FEBS Lett.* **331,** 134–140.
5. Stöcker, W., Grams, F., Baumann, U., Reinemer, P., Gomis-Rüth, F. X., McKay, D. B. & Bode, W. (1995) *Protein Sci.* **4,** 823–840.
6. Gomis-Rüth, F. X., Kress, L. F. & Bode, W. (1993) *EMBO J.* **12,** 4151–4157.
7. Gomis-Rüth, F. X., Kress, L. F., Kellermann, J., Mayr, I., Lee, X., Huber, R. & Bode, W. (1994) *J. Mol. Biol.* **239,** 513–544.
8. Wolfsberg, T. G. & White, J. M. (1996) *Dev. Biol.* **180,** 389–401.
9. Black, R. A., Durie, F. H., Otten-Evans, C., Miller, R., Slack, J. L., Lynch, D. H., Castner, B., Mohler, K. M., Gerhart, M., Johnson, R. S., *et al.* (1996) *Biochem. Biophys. Res. Commun.* **225,** 400–405.
10. Mohler, K. M., Sleath, P. R., Fitzner, J. N., Cerretti, D. P., Alderson, M., Kerwar, S. S., Torrance, D. S., Otten-Evans, C., Greenstreet, T., Weerawarna, K., *et al.* (1994) *Nature (London)* **370,** 218–220.
11. DiMartino, M., Wolff, C., High, W., Stroup, G., Hoffman, S., Laydon, J., Lee, J. C., Bertolini, D., Galloway, W. A., Crimmin, M. J., *et al.* (1997) *Inflamm. Res.* **46,** 211–215.
12. Crowe, P. D., Walter, B. N., Mohler, K. M., Otten-Evans, C., Black, R. A. & Ware, C. F. (1995) *J. Exp. Med.* **181,** 1205–1210.
13. Moreland, L. W., Baumgartner, S. W., Schiff, M. H., Tindall, E. A., Fleischmann, R. M., Weaver, A. L., Ettlinger, R. E., Cohen, S., Koopman, W. J., Mohler, K., *et al.* (1997) *N. Engl. J. Med.* **337,** 141–147.
14. Otwinowski, Z. & Minor, W. (1993) *DENZO: A Film Processing for Macromolecular Crystallography* (Yale University, New Haven, CT).
15. Otwinowski, Z. (1991) in *Isomorphous Replacement and Anomalous Scattering, Daresbury Study Weekend Proceedings* (SERC Daresbury Laboratory, Warrington, U.K.).
16. Cowtan, K. (1994) *Joint CCP 4 ESF-EACBM Newsletter on Protein Crystallography* **31**.
17. Roussel, A. & Cambilleau, C. (1989) *turbo-frodo in Silicon Graphics Geometry*, Partners Directory (Silicon Graphics, Mountain View, CA).
18. Brünger, A. T. (1991) *Curr. Opin. Struct. Biol.* **1,** 1016–1022.
19. Collaborative Computational Project Number 4. (1994) *Acta Crystallogr.* **D50,** 760–763.
20. Evans, S. V. (1993) *J. Mol. Graph.* **11,** 134–138.
21. Gomis-Rüth, F. X., Maskos, K., Betz, M., Bergner, A., Huber, R., Suzuki, K., Yoshida, N., Nagase, H., Brew, K., Bourenkov, G. P., *et al.* (1997) *Nature (London)* **389,** 77–81.
22. Nicholls, A., Bharadwaj, R. & Honig, B. (1993) *Biophys. J.* **64,** A166.
23. Rosendahl, M. S., Ko, S. C., Long, D. L., Brewer, M. T., Rosenzweig, B., Hedl, E., Anderson, L., Pyle, S. M., Moreland, J., Meyers, M. A., *et al.* (1997) *J. Biol. Chem.* **272,** 24558–24593.
24. Grams, F., Reinemer, P., Powers, J. C., Kleine, T., Pieper, M., Tschesche, H., Huber, R. & Bode, W. (1995) *Eur. J. Biochem.* **228,** 830–841.
25. Tang, P., Hung, M.-C. & Klostergaard, J. (1996) *Biochemistry* **35,** 8216–8225.
26. Tang, P., Hung, M.-C. & Klostergaard, J. (1996) *Biochemistry* **35,** 8226–8233.
27. Perez, C., Albert, I., DeFay, K., Zachariades, N., Gooding, L. & Kriegler, M. (1990) *Cell* **63,** 251–258.
28. Jones, E. Y., Stuart, D. I. & Walker, N. P. C. B. (1989) *Nature (London)* **338,** 225–228.
29. Zhang, D., Botos, I., Gomis-Rüth, F. X., Doll, R., Blood, C., Njoroge, F. G., Fox, J. W., Bode, W. & Meyer, E. F. (1994) *Proc. Natl. Acad. Sci. USA* **91,** 8447–8451.
30. Kumasaka, T., Yamamoto, M., Moriyama, H., Tanaka, N., Sato, M., Katsube, Y., Yamakawa, Y., Omori-Satoh, T., Iwanaga, S. & Ueki, T. (1996) *J. Biochem.* **119,** 49–57.
31. Lunn, C. A., Fan, X., Dalie, B., Miller, K., Zavodny, P. J., Narula, S. W. & Lundell, D. (1997) *FEBS Lett.* **400,** 333–335.
32. Pan, D. & Rubin, G. M. (1997) *Cell* **90,** 271–280.
33. Hooper, N. M., Karran, E. H. & Turner, A. J. (1997) *Biochem. J.* **321,** 265–279.